Pol. J. Environ. Stud. Vol. 33, No. 6 (2024), 6015-6024
DOI: *10.15244/pjoes/173446* ONLINE PUBLICATION DATE: 2024-07-10

Review

Delineating Pixels of Natural Hydrocarbon Micro-Seepage Induced Alterations and Anomalies in Overlying Soils and Sediments in Ugwueme, with ASTER Data and Band Ratio Technique

Mfoniso Asuquo Enoh[1*], Ojanikele Willie Augustine[2], Ndukwe Emmanuel Chiemelu[1], Stephen Eguba Ekwok[3], Anthony E. Akpan[3], Ahmed Eldosouky[4], Saad S. Alarifi[5], Peter Andras[6]**

[1]Department of Geoinformatics and Surveying, University of Nigeria, Enugu, Nigeria
[2]Department of Surveying and Geoinformatics, Delta State University of Science and Technology, Ozoro, Delta State, Nigeria
[3]Applied Geophysics programme, Department of Physics, University of Calabar, Calabar, Nigeria
[4]Geology Department, Faculty of Science, Suez University, Suez, 43221, Egypt, dr_a.eldosoky@yahoo.com, ORCID ID: https://orcid.org/my-orcid?orcid=0000-0003-1928-9775
[5]Department of Geology & Geophysics, College of Science, King Saud University, Saudi Arabia ssalarifi@ksu.edu.sa
[6]Faculty of Natural Sciences, Matej Bel University in Banska Bystrica, Tajovského 40, 974 01 Banska Bystrica, Slovakia, peter.andras@umb.sk

Received: 19 February 2023
Accepted: 6 October 2023

Abstract

The earth's underlying hydrocarbon-bearing reservoirs frequently leak. These reservoirs leak because of their inadequate sealing, and at high pressure, oil and gas escape vertically or nearly vertically to the earth's surface as seepage. Micro-seepages on the earth's surface cause oxidation-reduction reactions, which cause anomalies in the soils and sediments beneath them. Remote sensing (RS) and geographic information systems (GIS) are important tools for investigating hydrocarbon micro-seepage-induced changes and anomalies in overlying soil and sediments. In this study, ASTER remote sensing data was adopted to delineate pixels of hydrocarbon micro-seepage-induced anomalies in Ugwueme, south-eastern Nigeria. Band Ratio (BR) was used as a spectral enhancement technique to detect alterations and anomalies in the overlying soil and sediments. ASTER BR of 2/1 improves ferric iron; (5+7)/6 improves clay minerals; (1+4)/(2+3) improves ferrous iron; and 4/(6+9) improves gypsum.

*e-mail: enohmfoniso@yahoo.com;
**e-mail: emmanuel.chiemelu@unn.edu.ng

The study highlights that BR is an excellent spectral enhancement technique for delineating areas of alterations and anomalies induced by hydrocarbon micro-seepage.

Keywords: alterations, anomalies, ASTER data, band ratio, hydrocarbon micro-seepage

Introduction

The earth's underground petroleum reservoirs are often saturated with oil and gas, concealed within the earth's impermeable reservoir [1-5]. As a result of differences in pressure, these oil and gas leaks migrate vertically or nearly vertically along geological faults, fractures, and layers of rocks to shallow levels and finally to the earth's surface as seepages [6-9] (Fig. 1). The vertical movement of oil and gas through geological faults and fractures and within the sub-surface bedding plane is known as the "chimney effect" [10-13]. Through its passage, the chimney effect often generates oxidation-reduction reactions that produce anomalies in overlying soils and sediments. Microbial and mineralogical anomalies, as well as changes in the electrical and magnetic characteristics, often occur at the near surface and on the surface of overlying sediments and soils [14-17]. Among these anomalies and alterations, red bed bleaching (conversion of Fe^{3+} to Fe^{2+}) [18-20], clay minerals (conversion of feldspar to clay minerals, such as kaolinite) [21-23], carbonates (the presence of Fe^{2+} rich carbonates, such as siderite), [24-27], and ferrous iron enrichment [28-30] often express diagnostic spectral characteristics, which can be detected and interpreted with remote sensing technology [31-33]. The description of these anomalies and alterations as represented in Fig. 1 is highlighted as follows [8, 34-36]:

(a) Red bed bleaching: Red beds or sediments often appear reddish if they contain iron oxide (hematite). When hydrocarbon seepage comes into contact with reddish sediments, it degrades the iron oxide and bleaches them. Bleached sediments frequently include more siderite and pyrite and less ferric iron [37-39].

(b) Clay mineral precipitation: In areas of hydrocarbon micro-seepage, clay minerals like illite and smectite frequently transform into kaolinite. Kaolinite-rich sandstone exhibits brighter values in the band ratio image [40-42].

(c) Prevalent carbonate minerals: Carbonate minerals are created when calcium or magnesium oxides present in sediments react with carbon dioxide emerging from micro-seepage. As a result, carbonate mineral concentrations rise in micro-seepage milieus. The calcium and magnesium content of the parent materials, in contrast, governs the development of carbonate minerals [43-45].

(d) Present of magnetic minerals: The synthesis of ferrous minerals is stimulated by reducing the ferric iron level in a micro-seepage-impacted environment. The precipitation of pyrrhotite, magnetite, greigte, and maghemite has been observed in numerous hydrocarbon micro-seepage fields [46-48].

Hydrocarbon seepage found on the earth's surface may be macro- or micro-seepage [7, 49, 50]. Etiope [14] documented that Link [51] was the first scientist to have distinguished hydrocarbon seepage as either micro-seepage or macro-seepage. According to Etiope [14], macro-seepages are the visible onshore or offshore manifestations of oil, gas, and mud volcanoes, whereas micro-seepages are the invisible remains of light hydrocarbons that cause mineral alterations [52-54]. They are dominated majorly by methane (CH_4) and lightly by ethane (C_2H_6), propane (C_3H_8), butane (C_4H_{10}), and pentane (C_5H_{12}) gases [55-57]. At the surface, these hydrocarbon gases interact with the environment and produce mineralogical and botanical anomalies [58-60]. Long-term contact of hydrocarbon micro-seepage with overlying soils and sediments often alters their mineral composition, thereby producing changes in their pH, mineralogy, chemical, and physical properties [61-63]. These changes are manifested by changes in the color, hardness, radioactivity, magnetic, and electric properties of the rock minerals [64, 65]. Long-term exposure to hydrocarbon micro-seepage in the soil and sediments often results in local anomalous redox zones, which promote a wide range of mineral and chemical changes [66, 67]. Another important form of hydrocarbon seepage is active and passive seepage [52]. While active hydrocarbon seepage is associated with the subsurface, where oil and gas leak in large quantities into shallow soils and sediments as well as into the overlying water column, passive hydrocarbon seepage refers to areas or zones where subsurface oil and gas are inactively seeping [68-70]. Globally, hydrocarbon oil and gas seeps, and their diverse surface expressions are seen in sedimentary basins that contain oil and gas reserves [71-73].

The traditional techniques for studying hydrocarbon micro-seepage-induced alterations in soil and sediment have been extensively studied. These techniques, which include geophysical and geochemical analyses, are expensive, time-consuming, and destructive, and they are only suitable for selected observations within the vicinity of drilling sites in active oil fields [74-77]. Remote sensing offers a quick, cheap, and non-destructive solution for studying hydrocarbon micro-seepage manifestations at or near the earth's surface [54, 78]. Although remote sensing techniques cannot directly identify micro-seepage, they can detect patterns of large-scale modification [59, 68]. In the past few decades, researchers have employed spectral enhancement techniques such as false color composite (FCC), band ratio (BR), and principal component analysis (PCA) to identify areas of surface-based alterations and anomalies induced by hydrocarbon micro-seepage on soil and sediments [79, 80].

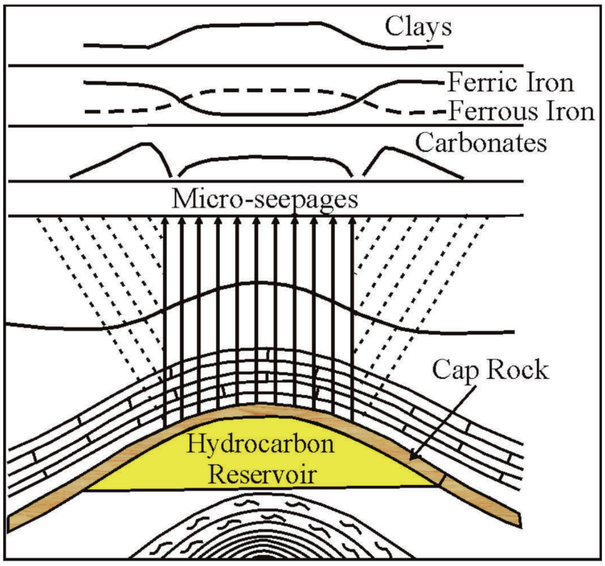

Fig. 1. Hydrocarbon micro-seepage model (modified from [71]).

In this study, the overall aim was to apply the BR algorithm and Advanced Space-borne Thematic Emission and Reflection Radiometer (ASTER) data to delineate pixels of mineral alterations and anomalies induced by natural hydrocarbon micro-seepage in Ugwueme. Field observation is an integral part of the study. Fieldwork was carried out in the study area to ascertain the hydrocarbon micro-seepage-prone zone.

ASTER is a multispectral sensor found on the Earth's Observing System (EOS) Terra platform that measures electromagnetic radiation from the surface in 14 bands [81-84]. Case studies by Salati et al. [85], Rowan et al. [86], Poumandari et al. [87], and Rockwell et al. [88] have shown that ASTER data has successfully been used to delineate pixels of alterations and anomalous minerals by utilizing their emissivity, absorption, and reflection features in the SWIR and TIR regions of the electromagnetic spectrum [86, 89]. Ugwueme is a developing town situated in Enugu, in the southeastern part of Nigeria. The area is cited as being on fairly elevated terrain, covering an area of about 82 km on a scale of 1 to 25, 000 km [90, 91]. Ugwueme is accessible by a laterite road and can be found between latitudes 6°0‘00”N and 6°07‘00”N and longitudes 7°24‘00”E and 7°30‘00” E in geographic coordinates [8, 92].

Materials and Methods

Description of the Study Area

The study area "Ugwueme" is situated on a fairly leveled elevation between latitudes 6°0‘00” N and 6°07‘00” N and longitudes 7°24‘00” E and 7°30‘00”E in Enugu, South-Eastern Nigeria. The region falls under the Tropical Wet and Dry Climate "AW" of the Koppen climate classification scheme [3, 6]. The wet season lasts from April to September, while the dry season runs from November to March of the following year. The dry season is characterized by little rainfall, high sunshine, and dryness. During the wet season, Ugwueme experiences heavy rainfall, with a record of 1,800 mm, which results in significant floods, soil leaching, erosion, severe outwash, groundwater penetration, and percolation. According to studies, this climatic circumstance is thought to be the primary reason for the oil seepage that flushed out from the tar sand as heavy, viscous, and sticky crude within the study area [3, 6]. The temperature is high in the area, and during the dry weather, it rises up to 26.6ºC.

Geological Settings of the Study Area

The geological setting of Ugwueme is explained in the study geology map (Fig. 2). The study area and its environs are underlain by four formations and five main lithological facies. These formations are the Awgu Shale, Owelli Sandstone, Mamu, and Ajali Formations. The main lithological facies associated with the study area are the heterolith sediments, dark gray shale, coarse grain, medium grain, and whitish cross-bedded sandstones [92, 93]. The Awgu shale is documented to be up to 300 ft. thick. The formation is made of bluish-gray, well-bedded shale with occasional intercalations of yellow, pale, fine-grained sandstones and thin-shell limestone [3, 94]. The Owelli sandstones are mostly ferruginous and are characterized as medium-to-coarse-grained sandstones [3, 93]. Toward the Awgu location, the Owelli sandstone is estimated to be 250 m thick. At the oil and gas seepage spot, situated in Ugwueme, the Owelli sandstone is assumed to be about 130 m thick, resting conformably on the Awgu shale [52, 93]. The Mamu Formation (Lower Coal Measures)

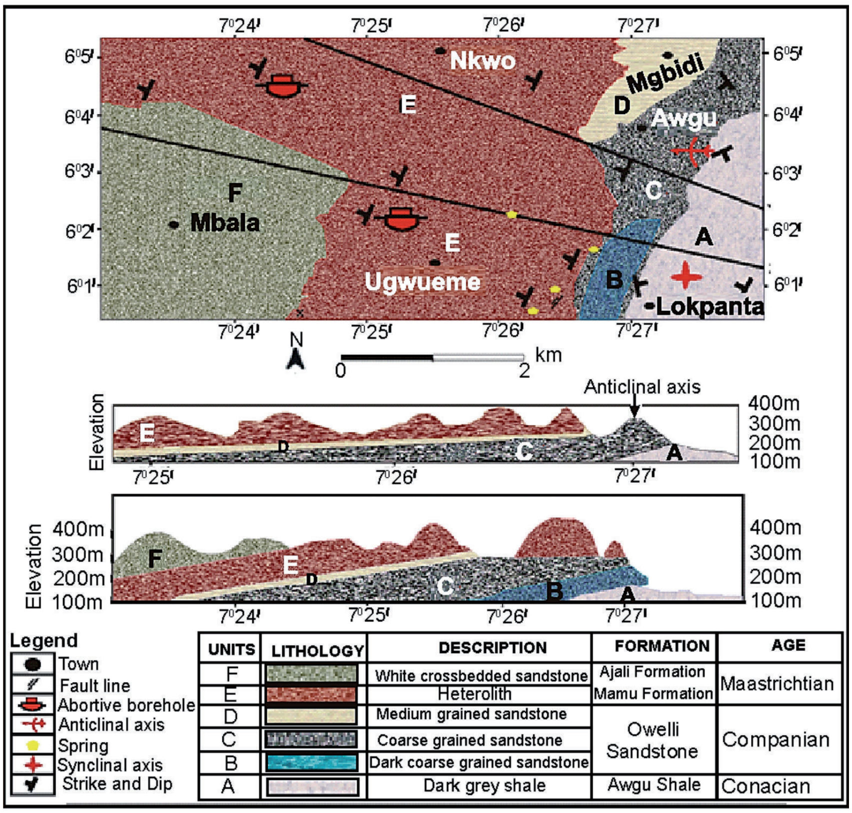

Fig. 2. Geology map of Ugwueme.

is dated from the Lower to Middle Maastrichtian and is between 100 m and 1000 m thick. These formations are characterized by the alternation of coal seams with sandstone, siltstone, mudstone, and rare shale. The Ajali Formation is composed of friable and thick medium- to coarse-grain sandstones that are poorly sorted and whose conformability is above that of the Mamu Formation [92].

Data Sources and Pre-Processing

ASTER is a one-of-a-kind sensor that records electromagnetic radiation in 14 district bands with 15-m, 30-m, and 90-m spatial resolutions in the visible-near infrared (VNIR), shortwave infrared (SWIR), and thermal infrared (TIR) (Table 1) [95-97]. With a spatial resolution of 15 m, 30 m, and 90 m, the sensor has three VNIR bands ranging from 0.52 µm to 0.86 µm, six SWIR bands ranging from 1.60 µm to 2.43 µm, and five TIR bands ranging from 8.125 µm to 11.65 µm. The wavelength areas of VNIR, SWIR, and TIR offer spectral resolution concerning rocks and minerals [98, 99]. The VNIR area of the ASTER sensor is very effective in detecting iron-oxide minerals containing Fe^{2+} or Fe^{3+} ions. Altered rocks and minerals containing hydroxyl (OH) and carbonate (CO_3), such as Al-OH, Fe-OH, Mg-OH, and carbonate minerals, exhibit different absorption signatures in the SWIR region. The Earth Resources Observation and Science (EROS) Center in the United States and the Earth Remote Sensing Data Analysis Center (ERSDAC) in Japan offer ASTER products

Table 1. Band specification of the ASTER sensor [87, 89].

Subsystem	Band No.	Spectral Range (µm)	Spatial Resolution (m)
VNIR	1	0.52–0.60	15
	2	0.63–0.69	
	3N	0.78–0.86	
	3B	0.78–0.86	
SWIR	4	1.60–1.70	30
	5	2.145–2.185	
	6	2.185–2.225	
	7	2.235–2.285	
	8	2.295–2.365	
	9	2.360–2.430	
TIR	10	8.125–8.475	90
	11	8.475–8.825	
	12	8.925–9.275	
	13	10.25–10.95	
	14	10.95–11.65	

[100-102]. Two ASTER preprocessing approaches are cross-talk correction of ASTER-SWIR bands and layer stacking of VNIR-SWIR bands into a unique nine-band data cube. The cross-talk phenomenon has a tremendous impact on the ASTER-cross-talk SWIRs. This phenomenon changes radiance measurements within the SWIR area as a result of ASTER's instrumental difficulties, resulting in deceptive reflectance spectra and mineral misidentification [103, 104]. Crosstalk can be decreased by utilizing the crosstalk correction program at www.gds.aster.ersda.c.or.jp. To convert pixel radiance within the sensor into the reflectance of the surface data, the ENVI (Environment for Visualizing Images) version 5.1 software's rapid line of sight atmospheric analysis of spectral hypercubes (FLAASH) module and thermal atmospheric correction of ASTER TIR emittance bands were used [105, 106].

Methods

To give the anomalous surface mineral assemblages more prominence in the study, the subset images were processed with the band ratio (BR) technique in order to delineate pixels of mineral anomalies and alterations. Band-rationing (BR) is a useful remote sensing technique for identifying spectral changes in minerals [80, 89]. It's a multispectral image analysis that involves dividing one spectral image band by another in arithmetic terms [16, 58, 107]. The ratio of spectral reflectance measured in one spectral image band to spectral reflectance measured in another spectral image band is the outcome of this arithmetic division [62, 108]. After removing atmospheric factors such as haze from the image, band rationing improves the contrast between the objects by dividing the brightness values at peaks and troughs in a reflectance curve. Compositional information is enhanced through spectral band rationing, whereas other sorts of information about the earth's surface are suppressed. This approach is great for emphasizing characteristics or materials. Equation (1) depicts the basic equation for calculating the band ratio technique [52, 109].

$$B_R = (B_1)_i / (B_2)_j \quad (1)$$

Where B_1 and B_2 represent the specific image bands, while i and j denote the digital numbers (DN) situated in the bands. In this study, band ratios (BR), an important spectral enhancement technique, were calculated using various bands in ASTER data to improve the spectral signatures of alteration and anomalous minerals [63]. ASTER BR of 2/1 enhances ferric iron [85]; (5+7)/6 enhances clay minerals [110], after [51]; (1+4)/(2+3) enhances ferrous iron [88]; and 4/(6+9) enhances gypsum [85].

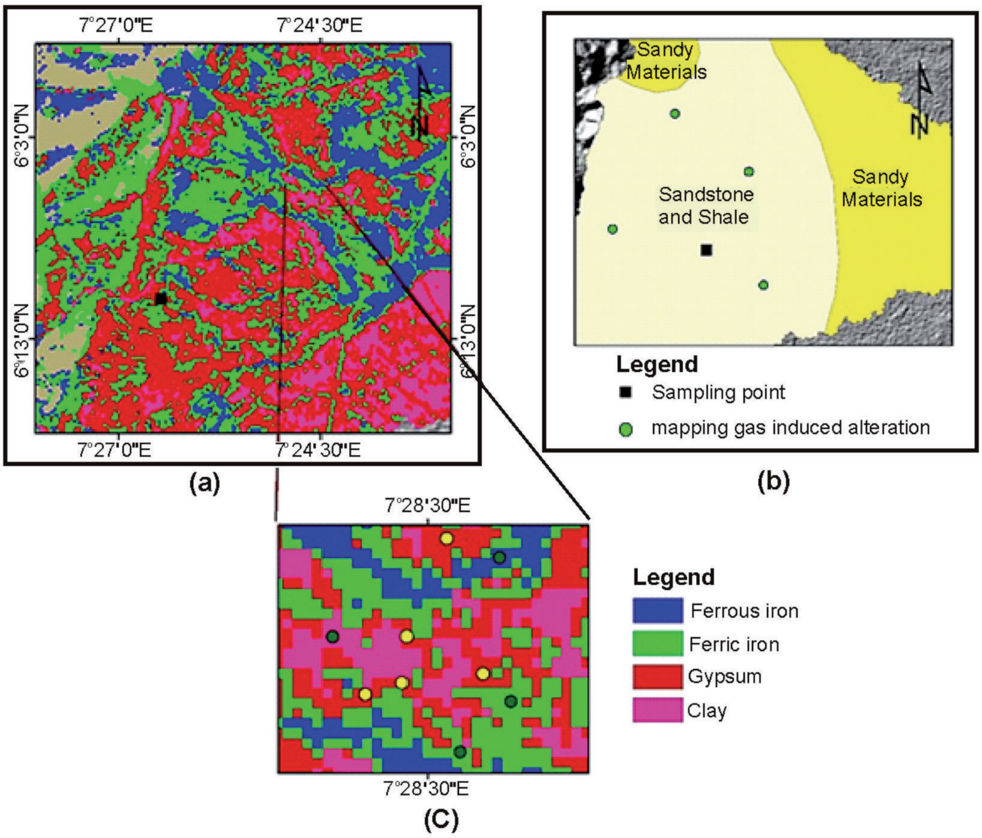

Fig. 3. a) False color composite (FCC) map, formed by the BR images; b) Alteration zones elucidated in the study geology map. c) BR of 2/1 enhances ferric iron; (5 + 7)/6 enhances clay minerals; (1+4)/(2+3) enhances ferrous iron; and 4/(6 + 9) enhances gypsum.

Results and Discussion

Fig. 3a) shows the false color composite (FCC) map. The FCC maps in the study are formed by the BR images to indicate ferric iron, ferric oxides, gypsum, and clay minerals as channels of red (R), green (G), and blue (B), respectively. The alteration zones are represented by small spheres, as shown in Fig. 3b), and are highlighted in green. The field sample measurement is represented by a small, dark-colored square, which is elucidated in the study geological map. Fig. 3c) depicts the enlarged portion of the FCC map that clearly distinguishes ferric iron, clay minerals, ferrous iron, and gypsum mineralogical alterations with band ratio index. Their description is highlighted below:

Ferric iron index: Ferric iron minerals exhibit high reflectance at ASTER band 2 and broad absorption at the NIR wavelength (ASTER band 1). To depict ferric iron mineral pixels in the study area, the ASTER band ratio index of 2/1 is employed. In this study, the FCC of the band ratio, which displays ferric iron, is green.

Clay mineral index: Clay minerals frequently exhibit high reflectance abilities in ASTER bands 5 and 7, as well as vibrational Al-OH absorption characteristics in band 6. In addition to this, clay-bearing locations within the study area were delineated with ASTER BR (5+7)/6. In the study, clay pixels are highlighted in pink.

Ferrous iron index: Ferrous iron materials have high reflectance properties at ASTER bands 1 and 4 as well as an absorption feature in the VNIR wavelength of ASTER bands 2 and 3. To depict ferrous minerals in the study area, the ASTER BR (1+4)/(2+3) is employed. In the study, ferrous iron is delineated with a blue color.

Gypsum index: Gypsum displays high reflectance at ASTER band 4 and absorption at ASTER bands 6 and 9. Thus, in the study, ASTER BR 4/(6+9) is utilized to discriminate gypsum, with a red color from the study area background pixels.

Conclusions

Remote sensing is a useful technique for analyzing and modeling hydrocarbon micro-seepage-impacted areas. The technique is cheap, rapid, and non-destructive, and it can be used to delineate areas of mineralogical and botanical anomalies. Anomalies and alterations in soil and sediment can be found on the earth's surface in a variety of ways. Within these forms, red bed bleaching, ferrous iron enrichment, clay minerals, and carbonate alterations exhibit abnormal spectral signatures, which can be analyzed with remote sensing tools. In this study, the band ratio (BR) algorithm was the technique used with the ASTER sensor to delineate areas of surface mineral alterations and anomalies induced by hydrocarbon micro-seepage in Ugwueme. ASTER BR of 2/1 enhances ferric iron; (5+7)/6 enhances clay minerals; (1+4)/(2+3) enhances ferrous iron; and 4/(6+9) enhances gypsum. The study highlights that BR is an excellent spectral enhancement technique for delineating areas of alterations and anomalies induced by hydrocarbon micro-seepage.

Acknowledgments

1. The authors are grateful to the USGS forsupplying the ASTER dataset.
2. This research was supported by Researchers Supporting Project number (RSP2024R496), KingSaud University, Riyadh, Saudi Arabia.

Conflict of Interest

The authors declare no conflict of interest.

References

1. ASADZADEH S., CARLOS R. Characterization of microseepage-induced diagenetic changes in the upper red formation, Qorn region, Iran I. Outcrop, geochemical, and remote sensing studies. Marine and Petroleum Geology, **117**, 1, **2020**.
2. RASHEED M.A., LAKSHMI M., RAO P.L.S., KALPANA M.S., DAYAL A.M., PATIL D.J. Geochemical evidences of trace metal anomalies for finding hydrocarbon micro-seepage in the petroliferous regions of Tatipaka and Pasarlapudi areas of Krishna Godavan Basin, India Petroleum Science Journal, **10**, 19, **2013**.
3. ENOH M.A., ONWUZULIGBO C., NARINUA N.Y. Stimulating the impact of hydrocarbon micro-seepage on vegetation in Ugwueme from 1996 to 2030, based on the Leaf Area Index and Markov Chain Model. Engineering Proceedings, **31** (1), 47, **2023**.
4. YANG D., QIU H., YE B., LIU Y., ZHANG J., ZHU Y. Distribution and Recurrence of Warming-induced Retrogressive Thaw Slumps on the Central Qinghai-Tibet Plateau. Journal of Geophysical Research: Earth Surface, 128 (8), **2023**.
5. DAI Z., MA Z., ZHANG X., CHEN J., ERSHADNIA R., LUAN X., SOLTANIAN M.R. An integrated experimental design framework for optimizing solute transport monitoring locations in heterogeneous sedimentary media. Journal of Hydrology, **614**, 128541, **2022**.
6. ENOH M.A., OKEKE F.I., OKEKE U.C. Automatic Lineaments mapping and extraction in relationship to natural hydrocarbon seepage in Ugwueme, South-Eastern Nigeria. Geodesy and Cartography, **47** (1), 33, **2021**.
7. ZHENG G., XU W., ETIOPE G., XIANGXIAN M., SHOUYUN L., QIAOHUI F., WASIM S., YANG L. Hydrocarbon seeps in petroliferous basins in China. A first inventory. Journal of Asian Earth Sciences, **151**, 269, **2018**.
8. XU Z., WANG Y., JIANG S., FANG C., LIU L., WU K., LUO Q., LI X., CHEN Y. Impact of input, preservation and dilution on organic matter enrichment in lacustrine rift basin: A case study of lacustrine shale in Dehui Depression of Songliao Basin, NE China. Marine and Petroleum Geology, **135**, 105386, **2022**.

9. XU Z., LI X., LI J., XUE Y., JIANG S., LIU L., LUO Q., WU K., ZHANG N., FENG Y., SHAO M., KEXIN J., SUN Q. Characteristics of Source Rocks and Genetic Origins of Natural Gas in Deep Formations, Gudian Depression, Songliano Basin, NE China. ACS Earth and Space Chemistry, **6** (7), 1750, **2022**.
10. SHI P.L., FU B.H., NINOMIYA Y. Detecting lithology features from ASTER VNIR-SWIR multispectral data in the arid region: A case study in the eastern Kalpin uplift, southwest Tian Shan. Chinese Journal of Geology, **45** (1), 333, **2010**.
11. ZHANG T., SONG B., HAN G., ZHAO H., HU Q., ZHAO Y., LIU H. Effects of coastal wetland reclamation on soil organic carbon, total nitrogen and total phosphorus in China: A meta-analysis. Land Degradation & Development, **34** (11), 3340, **2023**.
12. LI W., SHI Y., ZHU D., WANG W., LIU H., LI J., SHI N., MA L., FU S. Fine root biomass and morphology in a temperate forest are influenced more by the nitrogen treatment approach than the rate. Ecological Indicators, **130**, 108031, **2021**.
13. ZHENG Z., ZUO Y., WEN H., LI D., LUO Y., ZHANG J., YANG M., ZENG J. Natural gas characteristics and gas-source comparisons of the lower Triassic Feixianguan formation, Eastern Sichuan Basin, China, Petroleum Science, **20** (3), 1458, **2023**.
14. ETIOPE G. Natural gas seepage. The Earth's Hydrocarbon Degassing, Springer, **640**, **2015**.
15. HE M., DONG J., JIN Z., LIU C., XIAO J., ZHANG F., SUN H., ZHAO Z., GOU L., LIU W., LUO C., SONG Y., MA L., DENG LI. Pedogenic processes in loess-paleosol sediments: Clues from Li isotopes of leachate in Luochuan loess. Geochimica et Cosmochimica Acta, **299**, 151, **2021**.
16. JIA B., ZHOU G. Estimation of global karst carbon sink from 1950s to 2050s using response surface methodology. Geo-spatial Information Science, 1, **2023**.
17. WEI X., BAI X., WEN X., LIU L., XIONG J., YANG C. A large and overlooked Cd source in Karst areas. The migration and origin of Cd during soil formation and erosion, Science of the Total Environment, **895**, 165126, **2023**.
18. RASHEED M.A., LAKSHMI M., RAO P.L.S., KALPANA M.S., DAYAL A.M., PATIL D.J. Geochemical evidences of trace metal anomalies for finding hydrocarbon microseepage in the petroliferous regions of Tatipaka and Pasarlapudi areas of Krishna Godavari Basin, India. Petroleum Science, **10** (1), 19, **2013**.
19. BHAGOBATY R.K. Hydrocarbon-utilizing bacteria of natural crude oil seepages, Digboi oilfield Northern region of India. Journal of Sedimentary Environments, **5** (2), 177, **2020**.
20. BORUAH A., VERMA S., RASHEED A., GAIROLA G.S., GOGOI A. Macro-seepage based potential new hydrocarbon prospects in Assam-Arakan Basin, India. Scientific Reports, **12** (1), 2273, **2022**.
21. SHAGAPOV V.S., BASHMAKOV R.A., FOKEEVA N.O., SHAMMATOVA A.A. Evolution of filtration pressure waves in a Hydraulic Fracture during Transient-Well-Operation modes. Mathematics, **11** (1), 98, **2023**.
22. RASHEED M.A., LAKSHMI M., KALPANA M.S., PATIL D.J., DAYAL A.M. Recognition of hydrocarbon microseepage using microbial and adsorbed soil gas indicators in the petroliferous region of Krishna-Godavari Basin, India. Current Science, **112** (3), 560, **2017**.
23. SRINIVAS C., MADHAVI T., MUTNURI L., TIWARI D., KALPANAA M.S., PATIL D., DAYAL A.M., RAJU S.V. Geochemical characterization of adsorbed light gaseous alkanes in near surface soils of the eastern Ganga basin for hydrocarbon prospecting. Geochemistry International, **52** (1), 68, **2014**.
24. SECHMAN H., GUZY P., KASZUBA P., WOJAS A., MACHOWSKI G., TWAROG A., MASLANKA A. Direct and indirect surface geochemical methods in petroleum exploration: a case study from eastern part of the Polish Outer Carpathians. International Journal of Earth Sciences, **109** (5), 1853, **2020**.
25. SECHMAN H., IZYDOR G., GUZY P., DZIENIEWICZ M. Surface geochemical exploration for hydrocarbons in the area of prospective structures of the Lublin Trough (Eastern Poland). Marine and Petroleum Geology, **61**, 22, **2015**.
26. SCHUMACHER D. Minimizing Exploration Risk: The impact of hydrocarbon microseepage surveys for distinguishing hydrocarbon-charged traps from traps without hydrocarbons. In: AAPG Annual Convention and Exhibition, Houston, Texas, United States, **2017**.
27. VARJANI S.J. Microbial degradation of petroleum hydrocarbons. Bioresour Technology, **223**, 277, **2017**.
28. HOSSEINI A., SABERI M.H., ZARENEZHAD B. Significance of petroleum seepages in hydrocarbon exploration-case study of Khourian Desert, Central Iran. Petroleum Exploration and Production Technology, **12**, 1649, **2022**.
29. RADHA B.A., RASHEED M.A., RAO P.L.S., KALPANA M.S., DAYAL A.M. Light hydrocarbons Geochemistry of Surface Sediments from Pranhita-Godavari Basin, Andhra Pradesh. Geological Society of India, **78** (5), 477, **2011**.
30. LAKSHI M., RASHEED M.A., REDDY B., MADHAVI T., KALPANA M., PATIL D.J., DAVAL A.M. Light gasesous hydrocarbon studies in the near-surface soils of Tatipaka, Pasarlapudi and Kaza areas of Krishna-Godavari Basin, India. Current Science, **105** (3), 330, **2013**.
31. SHI P., FU B., NINOMIYA Y., SUN J., LI Y. Multispectral remote sensing mapping for hydrocarbon seepage-induced lithologic anomalies in the Kuqa foreland basin, south Tian Shan. Journal of Asian Earth Sciences, **46**, 70, **2012**.
32. FU B.H., ZHENG G.D., NINOMIYA Y., WANG C.Y., SUN G.Q. Mapping hydrocarbon-induced mineralogical alteration in the Northern Tian Shan using ASTER multispectral data. Terra Nova, **19** (4), 225, **2007**.
33. RASHEED M.A., PATIL D.J., DAYAL A.M. Microbial techniques for hydrocarbon exploration, Hydrocarbon, **2014**.
34. SCHUMACHER D. Hydrocarbon-induced alteration of soils and sediments. American Association of Petroleum Geologists, Memoir, **66**, 71, **1996**.
35. NING Z., HE Z., ZHANG S., YIN M., LIU Y., ZHANG C. Development of a prmA genes quantification technique and assessment of the technique's application potential for oil and gas reservoir exploration. Energy Exploration and Exploitation, **36** (5), 1172, **2018**.
36. SHU D., HE Y., YUE H., WANG Q. Metagenomic and quantitative insights into microbial communities and functional genes of nitrogen and iron cycling in twelve wastewater treatment systems. Chemical Engineering Journal, **290,** 21, **2016**.
37. KHAN S., JACOBSON S. Remote Sensing and Geochemistry for detecting hydrocarbon micro-seepages. Geological Society of America Bulletin, **120**, 96, **2008**.
38. SANTOSH G., DEBASHIS M., DAS P. Mapping hydrocarbon microseepage prospect areas by integrated studies of ASTER processing, geochemistry and

geophysical surveys in Assam-Arakan fold belt, NE India. International Journal of Applied Earth Observations and Geoinformation, 102432, **2021**.
39. XU K., TANG Y., REN C., ZHAO K., WANG W., SUN Y. Activity, distribution, and abundance of methane-oxidizing bacteria in the near surface soils of onshore oil and gas fields. Applied Microbiology and Biotechnology, **97** (17), 7909, **2013**.
40. MARS J.C., ROWAN L.C. Spectral assessment of new ASTER SWIR surface reflectance data products for spectroscopic mapping of rocks and minerals. Remote Sensing of Environment, **114** (9), 2011, **2010**.
41. LAMMAGLIA T., DE SOUZA, F., ROBERTO C. Unraveling hydrocarbon micro-seepage in onshore basins using spectral-spatial processing of advanced space borne thermal emission and reflection radiometer (ASTER) data. Surveys in Geophysics, **34** (3), 349, **2013**.
42. CAO X., SUN J., NING F., ZHANG H., WU N., YU Y. Numerical analysis on gas production from heterogeneous hydrate system in Shenhu area by depressurizing: Effects of hydrate-free interlayers. Journal of Natural Gas Science and Engineering, **101**, 104504, **2022**.
43. FENG S., DAN W., ZHANG X., SONG J., LI C., ZHOU S., CHEN S., REN J. Hydrocarbon accumulation conditions and distribution laws of Chang-2 reservior in Zhijing-Ansai area, China. Journal of Chengdu University of Technology (Science and Technology Edition), **47** (4), 451, **2020**.
44. HE Z., LI S., LIU Q., YANG T., ZHANG Y. Deep geological processes and deep resources in basins: Scientific issues and research directions. Petroleum Geology and Experiment, **42** (5), 767, **2020**.
45. LEONOV M.G., KERIMOV V.Y., MUSTAEV R.N., HAI V.N. The origin and mechanism of formation of hydrocarbon deposits of the Vietnamese shelf. Russian Journal of Pacific Geology, **14** (5), 387, **2020**.
46. LI C., LUO X., FAN C., ZHANG L., LIU A., LI H., LI J. Generation mechanism of overpressure and its implication for natural gas accumulation in Miocene reservoir in Ledong A structure, Ledong slope, Yinggehai Basin, Chinese Journal of Geology, **56** (4), 1034, **2021**.
47. XIE Y., LUO X., WANG D., XU C., XU Y., HOU M., CHEN A. Hydrocarbon accumulation of composite-buried hill reservoirs in the western subsag of Bozhong sag, Bohai Bay Basin. Natural Gas Industry B, **6** (6), 546, **2019**.
48. ZHANG Y., LUO J., ZHANG Y., HUANG Y., CAI X., YANG J., MAO D., LI J., TUO X., ZHANG Y. Resolution Enhancement for Large-Scale Real Beam Mapping Based on Adaptive Low-Rank Approximation. IEEE Transactions on Geoscience and Remote Sensing, **60**, 1, **2022**.
49. HIU G., CAO J., JIANG T. Discovery and prospecting significant of metal-bearing nanoparticles within natural invertebrate tissues. Ore Geology Reviews, **99** (5), **2018**.
50. SUN M., ZHANG P., ZHOU L., LIU H., LI G., CHEN J., TAN H., FANG X., YI Z., WANG G. Biomarker characteristics and oil accumulation period of Well Sutan 1 in Qaidam Basin, China. Journal of Natural Gas Geoscience, **1** (1), 85, **2016**.
51. LINK W.K. Significant of oil and gas seeps in world oil exploration. AAPG Bulletin, **36**, 1505, **1952**.
52. ENOH M.A., OKEKE U.C., BARINUA N.Y. Modelling and delineation of hydrocarbon micro-seepage prone zones on soils and sediments in Ugwueme, South Eastern Nigeria with Soil Adjustment Vegetation Index (SAVI). International Journal of Plant and Soil Science, **32** (13), 13, **2020**.
53. LILLESAND T.M., KIEFER R.W., CHIPMAN J.W. Remote Sensing and Image interpretation, 5th ed. John Wiley and sons Inc. New York. 763, **2004**.
54. MARTINELLI G., CREMONINI S., SAMONATI E. Geological and Geochemical setting of natural hydrocarbon emissions in Italy. Advances in Natural Gas Technology, 79, **2012**.
55. VAN DER MEER F.D., VAN DER WERFF H.M.A., VAN RUITENBEEK F.J.A., HECKER C.A., BAKKER W.H., NOOMEN M.F., VAN DER MEIJDE M., CARRANZA E.J., DE SMETH J.B., WOLDAI T. Multi- and Hyperspectral Geologic Remote Sensing. A Review. International Journal of Applied Earth Observation and Geoinformation, **14**, 112, **2012**.
56. BORUAH A. Integrated geo-microbial and trace metal anomalies for detection of hydrocarbon microseepage in Ahmedabad block of Cambay Basin, India. Journal of the Geological Society of India, **88**, 433, **2016**.
57. ZHANG C.Y., HE Z., ZHANG S., YIU M.Y., NING Z., LIU Y.C. A DNA based analysis of a microbial technique for the prospecting of oil and gas applied to a known oil field, China. Geomicrobiology, **34** (1), 63, **2017**.
58. GARAIN S., MITRA D., DAS P. Detection of hydrocarbon micro-seepage prospects using Landsat 8-based vegetation stress analysis in part of Assam-Arakan Fold Belt, NE India. Arabian Journal of Geosciences, **14** (1), **2021**.
59. ARGENTINO C., WAGHORN K.A., VADAKKEPULIYAMBATTA S., POLTEAU S., BUNZ S., PANIERI G. Dynamic and history of methane seepage in the SW Barents Sea: New insights from Leirdjupet Fault Complex. Scientific Report, **11** (1), 4372, **2021**.
60. ZHOU L., SUN Q., DANG X, WANG S. Comparison on multi-scale urban expansion derived from nightlight imagery between China and India. Sustainability, **11** (16), 4509, **2019V**
61. KENNICULT M. Oil and gas seeps in the Gulf of Mexico. In Habitats and Biota of the Gulf of Mexico: before the Deep water Horizon oil spill, ed. C Ward, New York Springer, pp. 275-358, **2017**.
62. AHMED S., AMIN B. Lithological mapping and hydrothermal alteration using Landsat 8 data: a case study in Ariab mining district, red sea hills, Sudan. International Journal of Basin and Applied Sciences, **3** (3), 199, **2014**.
63. ASADZADEH S., DE SOUZA FILHO ROBERTO C. Spectral remote sensing for onshore seepage characterization. A critical overview. Earth Science Reviews, **168**, 48, **2017**.
64. LIU R., CAO J., DENG Y., WANG G., LIU X. Formation of nana- or near nanoparticles via oxidation in the Dabaoshan concealed deposit, Guangdong Province. Arabian Journal of Geoscience, **13 (**20), **2020**.
65. LU M., CAO J., WANG Z., WANG G. Characteristics of naturally formed nanoparticles in various media and their prospecting significant in Chaihulanzi deposit. Minerals, **12** (10), 1289, **2022**.
66. HE J., ZHANG W., LU Z. Seepage system of oil-gas and its exploration in Yinggehai Basin located at Northwest of South China Sea. Journal of Natural Gas Geosciences, **2**, 29, **2017**.
67. MA S., QIU H., YANG D., WANG J., ZHU Y., TANG B., SUN K., CAO M. Surface multi-hazard effect of underground coal mining. Landslides, **20** (1), 39, **2023**.
68. SCHUMACHER D. Surface geochemical exploration for petroleum. Exploring for oil and gas traps. AAPG, Tulsa, **1999**.

69. LIU Y.Y., VAN DIJK A.I., DE JEU R.A.M., CANADELL J.G., MCCABE M.F., EVANS J.P., WANG G. Recent reversal in loss of global terrestrial biomass. Nature Climate Change, **5** (5), 470, **2015**.
70. RAO P.L.S., SRINU D., RASHEED M.A., KALPANA M.S., PATIL D. Correlation of trace elements with hydrocarbon micro-seepage. Journal of the Geological Society of India, **82** (6), 666, **2013.**
71. SCHUMACHER D.D. Surface geochemical exploration for oil and gas: New life for an old technology. The Leading Edge, **19**, 258, **2000**.
72. WANG Z., CAO J., QIU J., LIU X. Ore-forming elements and their distribution of nanoparticles in the updraft from the Sanshandao concealed deposit, China. Ore Geology Reviews, **138** (3), 104371, **2021**.
73. MOHAMMADI E. Sedimentary facies and depositional environments of the Oligocene-early Miocene marine Qom Formation, Central Iran Back-Arc Basin, Iran (northeastern margin of the Tethyan Seaway). Carbonates Evoporites, **35** (1), 1, **2020**.
74. KWANG C.E., DUKER A. Application of remote sensing and geographic information systems for gold potential mapping in Birim North of Eastern Region of Ghana. International Journal of Remote Sensing and Applications, **4** (1), 48, **2014**.
75. HABIB A., ABUZAR M.K., AHMAD I., SHAKIR U., MAHMOOD S.A., KHAN M.A., MAHMOOD M.F. Detection of mineral alteration induced by hydrocarbon micro-seepages by using remotely sensed data in the Fateh Jang area of the Northern Potwar region of Pakistan. Arabian Journal of Geosciences, **12**, 121, **2019**.
76. SADIYA T.B., IBRAHIM O., ASMA T.F, MAMFE V., NSOFOR C.J., OYEWMI A.S., SHAR J.T., SANUSI M., OZIGIS M.S. Mineral detection and mapping using band rationing and croasta technique in Bwari area council, Abuja, Nigeria. International Journal of Scientific and Engineering Research, **5** (12), 1100, **2014**.
77. MSHIU E.E., GLABER C., BORG G. Identification of hydrothermal paleofluid pathways, the pathfinders in the exploration of mineral deposits: A case study from the Sukuma land greenstone belt, Lake Victoria Gold field, Tanzania. Advances in Space Research, **55** (4), 1117, **2015**.
78. ZHOU Z. Fuzzy-based integration of Sentinal-2 MSI data for locating potential hydrocarbon microseepage. IOP Conference: Earth and Environmental Science, **783**, 012126, **2021**.
79. VAN DER MEER F.D., VAN DIJK P., VAN DER WERFF H. Remote Sensing and Petroleum Seepage: A Review and Case Study. Terra Nova, **14** (1), 1, **2002**.
80. LIU L., ZHOU J, HAN L., XU X.L. Mineral mapping and ore prospecting using Landsat TM and Hyperion data, Wushitala Xinjiang, Northwestern China. Ore Geology Review, **81**, 280, **2017**.
81. RAJENDRAN S., NASIR S. Characterization of ASTER spectral bands for mapping of alteration zones of volcanogenic massive sulphide deposits. Ore Geology Review, **88**, 317, **2017**.
82. AYOOBI I., TANGESTANI M.H. The effect of minimum noise fraction data input on success of artificial neural network in Lithological mapping of a magnetic terrain with ASTER data, a case study from SE Iran. Remote Sensing Applications Society and Environment, **7**, 21**, 2017.**
83. SULEMANA I.A., BALLARD J.Q., NTORI C., AWTWI A., ADEYINKA O.M., OKRAH T.M., ANSAH A.A. Location mapping of hydrothermal alteration using Landsat 8 data: A case of study in Prestea Huni Valley district, Ghana. International Journal of Geography and Geology, **9** (1), 13, **2020**.
84. POUR B.A., HASHIM M.A. Ali and Hyperion sensors data for lithological mapping and ore minerals exploration. Springer Plus, **3**, 130, **2014.**
85. SALATI S., VAN RUITENBEEEK F.V., VAN DER MEER F., NAIMI B. Detection of alteration induced by onshore gas seep from ASTER and WorldView-2 data. Remote Sensing, **6** (4), 3188, **2014.**
86. ROWAN L.C., SCHMIDT R.G., MARS J.C. Distribution of hydrothermally altered rocks in the Reko diq, Pakistan mineralized area based on spectral analysis of ASTER data. Remote Sensing of Environment, **104**, 74, **2006**.
87. POUMANDARI M., HASHIM M., POUR A.B. Spectral transformation of ASTER and Landsat TM bands for lithological mapping of Soghan ophiolite complex, South Iran. Advances in Space Research, **54** (4), 694, **2014**.
88. ROCKWELL B.W. Description and validation of an automated methodology for mapping mineralogy, vegetation, and hydrothermal alteration type from ASTER satellite imagery with examples from the San Juan Mountains, Colorando. U.S. Geological Survey Scientific Investigations Map, **35**, 3190, **2012**.
89. RAJENDRAN S., AL-KHIRBASH S., PRACEJUS B., NASIR S., AL-ABRI, AMANI H., KUSKY T.M., GHULAM A. ASTER detection of chromite bearing mineralized zones in Semail Ophiolite Massifs of the Northern Oman Mountains: Exploration strategy. Ore Geology Reviews, **44**, 121, **2012**.
90. OZODO D., ONYEABOR C. Water quality assessment of Ugwueme surface and ground water system. International Journal of Science and Research, **6** (9), 833, **2017**.
91. UBOCHI K.C., ABU N.E., NWADINIGWE A.O. Phenology of plant species found in Ugwueme hydrocarbon seep site, Enugu State, Nigeria. International Journal of Plant and Soil Science, **34** (22), 174, **2022**.
92. KOGBE C.A. The Cretaceous and Paleogene Sediments of Southern Nigeria. In Kogbe, C. A. Geology of Nigeria, Elizabeth Publishers, Lagos, 273, **1976**.
93. OBAJE N.G. Geology and Mineral Resources of Nigeria. Berlin: Springer, **2009**.
94. NWAJIDE C.S. Geology of Nigeria's Sedimentary Basin C.S.S. Bookshops Limited, **2013**.
95. ANDONGMA W.T., GAJERE J.N., AMUDA A.K., EDMOND R.R.D., FAISAL M., YUSUF Y.D. Mapping of hydrothermal alterations related to gold mineralization within parts of the Malumfashi Schist Belt, North-Western Nigeria. Egyptian Journal of Remote Sensing and Space Sciences, **24**, 401, **2021**.
96. REZAEI A., HASSANI H., MOAREFVAND P., GOLMOHAMMADI A. Lithological mapping in Sangan region in Northern Iran using ASTER satellite data and image processing methods, Geology, Ecology, and Landscape, **4** (1), 59, **2020**.
97. OTHMAN A.A., GLOAGEN R. Improving lithological mapping by SVM classification of spectral and morphological features: The discovery of a new chromite body in the Mawat ophiHolite complex (Kurdistan, NE Iraq). Remote Sensing, **6** (8), 6867, **2014**.
98. MASOUMI F., ESLAMKISH T., HONARMAND M., ABKAR A.A. A comparative study of Landsat-7 and Landsat 8 data using image processing methods for hydrothermal alteration mapping. Resource Geology, **67** (1), 72, **2017**.

99. WAMBO J.D.T., POUR A.B., GANNO S., ASIMOW P.D., ZOHEIR B., DOS REIS SALLES R, NZENTI J.P., PRADHAM B., MUSLIM A.M. Identifying high potential zones of gold mineralization in a sub-tropical region using Landsat-8 and ASTER remote sensing data: A case study of the Ngoura-Colomines goldfield, Eastern Cameroon. Ore Geology Reviews, **122**, **2020**.
100. ARIVAZHAGAN S., ANBAZHAGAN S. Aster data analysis for lithological discrimination of sittampundi Anorthositic complex, Southern India. Geoscience Research, **2** (3), 196, **2017**.
101. AMER R., KUSKY T., GHULAM A. Lithological mapping in the central eastern desert of Egypt using ASTER data. Journal of African Earth Sciences, **56**, 75, **2010**.
102. GOLMOHAMMADI A., KARIMPOUR M.H., MALEKZADEH S.A., MAZAHERI S.A. Alteration mineralization and radiometric ages of the source pluton at the sangan iron skarn deposit, northern Iran. Ore Geology Reviews, **65** (2), 545, **2014**.
103. REZAEI A., HASSANI H., MOAREFAVAND P., GOLMOHAMMADI A. Determination of unstable tectonic zones in C-North deposit, Sangan NE Iran using GPR method: Importance of structural geology. Journal of Mining and Environment, **10** (1), 177, **2019**.
104. SAHOO S., JHA M.K. Pattern recognition in lithology classification: Modeling using neural networks, self-organizing maps and genetic algorithms: Hydrology Journal, **25**, 311, **2016**.
105. VAN RUITENBEEK F.J.A., CUDAHY T.J., VAN DER MEER F.D., HALE M. Characterization of the hydrothermal systems associated with archean VMS mineralization at Panorama, Western Australia, using hyperspectral geochemical and geothermometric data. Ore Geology Reviews, **45**, 33, **2012**.
106. IWASAKI A., TONOOKA H. Validation of a crosstalk correction algorithm for ASTER/SWIR. IEEE Transactions on Geoscience and Remote Sensing, **43** (12), 2747, **2005**.
107. ALI A., POUR A.B. Lithological mapping and hydrothermal alteration using Landsat 8 data: A case study in Arab mining district, Red Sea Hills Sudan. International Journal of Sciences: Basic and Applied Research, **3**, 199, **2014**.
108. KAVAK K.S., CERTIN H. A detailed geologic lineament analysis using Landsat TM data of Golmarmara/Manisa Region, Turkey. Online Journal of Earth Sciences, **1** (3), 145, **2007**.
109. ZOHEIR B., EMAM A. Integrating geologic and satellite imagery data for high resolution mapping and gold exploration targets in the South Eastern Desert, Egypt. Journal of African Earth Sciences, **66**, 22, **2012**.
110. CROWLEY J.K., BRICKLEY D.W., ROWAN L.C. Airborne imaging spectrometer data of the Ruby Mountain, Montana: Mineral discrimination using relative absorption band-depth images. Remote Sensing of Environment, **29**, 121, **1989**.